PCCP

Accepted Manuscript

ROYAL SOCIETY OF CHEMISTRY

www.rsc.org/pccp

Physical Chemistry Chemical Physics
CREATED USING THE RSC LaTeX PCCP ARTICLE TEMPLATE – SEE www.rsc.org/electronicfiles FOR DETAILS
ARTICLE TYPE www. rsc.org/xxxxxx | XXXXXXXX

Thermal Phase Behavior and Ion Hopping in 1,2,4-Triazolium Perfluorobutanesulfonate Protic Organic Ionic Plastic Crystal†

Anirban Mondal,[a] Anurag Prakash Sunda[b] and Sundaram Balasubramanian*[a]

Received Xth XXXXXXXXXX 20XX, Accepted Xth XXXXXXXXX 20XX
First published on the web Xth XXXXXXXXXX 200X
DOI: 10.1039/b000000x

Critical aspects of thermal behavior and the electrolytic properties of solid-state Protic Organic Ionic Plastic Crystals (POIPCs) are unknown. We present molecular dynamics (MD) simulations on a perfect crystal and a vacancy model to probe such physical phenomenona in POIPC using 1,2,4-triazolium perfluorobutanesulfonate ([TAZ][pfBu]) as an example. Results show the existence of a rotator phase wherein the cations, although translationally ordered are disordered rotationally and exhibit a tumbling motion which significantly affects hydrogen bond lifetimes. van Hove correlation functions characterize concerted hopping of ions (cation or anion) at 500 K. These results are substantiated by calculated free energy barriers (for cation 2.5 kcal/mol and for anion 6 kcal/mol) and suggest that proton and ion transport influenced by the facile hydrogen bond dynamics in the rotator phase contribute to the solid-state conductivity of POIPC.

Keywords: Molecular Dynamics, phase transition, van Hove correlation function, free energy.

1 Introduction

The thermal phase behavior of organic ionic plastic crystals (OIPCs) is crucial for their potential applicability as solid electrolytes in batteries, fuel cells and dye-sensitized solar cells.[1–17] The occurrence of one or more than one solid–solid phase transition in such plastic crystals is yet another reason that draws one's attention to investigate their structural characteristics. The varying dynamics of ions in different solid phases contribute critically to the electrolytic properties of pristine and alkali metal doped OIPCs.[18–23] Recently, Jin et al.[7] investigated the ion transport mechanism in diethyl(methyl)(iso-butyl)phosphonium hexafluorophosphate ($[P_{1224}][PF_6]$) OIPC and showed that the tumbling motion of ions in its plastic phase aids in faster ion diffusion. Further, molecular dynamics (MD) simulations by Forsyth and coworkers[24,25] on $[P_{1224}][PF_6]$ showed the presence of dynamic heterogeneity in the solid phase and a crankshaft motion around the alkyl groups (methyl/ethyl group as head and the iso-butyl group as tail) in the plastic phase. Although plastic crystals exhibit long range translational order, orientational disorder can often set in at intermediate temperatures, which can enhance ion mobility.

Substantial progress has been made over the years in research on OIPCs to demonstrate their potential as solid-state anhydrous electrolytes.[4,9] However, a molecular-level understanding of the phase behavior, the temperature-dependent disordering phenomenon and transport mechanisms in Protic Organic Ionic Plastic Crystal (POIPC) materials is yet to be explored. While the dominant contribution to electrical conductivity is protonic, at moderate temperatures, ion motion too has been implicated[11]. Experiments on 1,2,4-triazolium perfluorobutanesulfonate ([TAZ][pfBu]) POIPC by Luo *et al.*[11] have revealed the following features: Up to 348 K, the crystal is stable, after which plastic deformation sets in. Ion rotation and likely diffusion happens in the range 350-375 K which is followed by a transition to a Phase-I (375-430 K) which exhibits high conductivity with an activation energy of 0.38 eV. In this phase, proton hopping via the Grotthuss mechanism is believed to be operative. Within a narrow range of temperature above 430 K, both cations and anions are also mobile which is followed by the melt phase. Given the above, details of the molecular motions of ions in the perfect crystal and of vacancies needs to be unravelled both by further experiments as well as microscopic simulations. While a study of proton transport is important, it will require *ab initio* MD simulations[26] and the likely inclusion of quantum effects on

† Electronic Supplementary Information (ESI) available: [Details of atomic site charge calculations, normal-mode analysis and estimation of ion hopping frequencies and jump diffusion coefficients are provided. Summary of cell parameters and non-exponential fit parameters for h-bond correlation functions are tabulated. Chemical structure of [TAZ][pfBu], change in volume with temperature, RDFs for various cation-anion sites, Powder XRD patterns, VDOS, MSD of cation and anion, reaction coordinate for free energy calculation and additional figures are shown.] See DOI: 10.1039/b000000x/

[a] *Chemistry and Physics of Materials Unit, Jawaharlal Nehru Centre for Advanced Scientific Research, Bangalore 560064, India.* [b] *Materials Research Laboratory, Department of Chemistry, Central University of Haryana, Mahendergarh, Haryana 123029, India. Fax: +91 (80) 2208 2766; Tel: +91 (80) 2208 2808; E-mail: bala@jncasr.ac.in*

dynamics. Using empirical potential MD simulations, one can, however gain an understanding of the nature of phases as well as mechanisms of vehicular diffusion of ions. In this spirit, in the present work, we report results on the structure of different thermal phases of 1,2,4-triazolium perfluorobutanesulfonate ([TAZ][pfBu]) POIPC, obtained using such classical MD simulations. Significant changes in the cation-anion hydrogen bonding network[11] and a concomitant freedom from orientational order is seen in the plastic crystalline phase of this compound.

2 Simulation Details

The chemical structure of [TAZ][pfBu] is presented in **Fig.** S1 of SI. MD simulations of the perfect crystalline phase of this salt and a model containing one ion pair vacancy were performed using LAMMPS program.[27] Initial cell parameters and atomic positions were taken from the experimentally determined crystal structure.[11] The size of simulation cell was 6x4x1 unit cells (2496 atoms). A description of the systems studied here is provided in **Table** S1 of Supporting Information (SI). The interaction parameters to model the triazolium cation were taken from the work of Maginn and co workers[28] and for the anion from the work of Goddard et al.[29] The latter force field did not have charges on sites which are crucial for the current study. Hence, the site charges on ions were determined via periodic density functional theory calculations performed using CP2K[30]. Results of such calculations yielded the valence electron density which was the input to the DDEC/c3 method to derive atomic site charges.[31,32] A distance cutoff of 12 Å was employed to calculate the pairwise interactions in real space. The time-step used to integrate the equations of motion was 0.5 fs. The long-range interactions were evaluated using PPPM solver with a precision of 10^{-5}. The calculated cell parameters at 100 K differed by less than 0.7% of their experimental values (See **Table** S2 of SI), which suggests that the crystal structure was stable in the simulations employing these force field parameters. Energy minimization was performed on the initial configuration. The configuration was then warmed to 300 K at a heating rate of 1 K/50 ps in the constant-NVT ensemble. It was followed by an equilibration of 5 ns at 300 K. The equilibrated configuration was further heated up to 500 K at a rate of 1 K/100 ps in the fully flexible isothermal-isobaric (NPT) ensemble. Coordinates were dumped each 10 K and a further equilibration of 4 ns was carried out in the fully flexible isothermal-isobaric (NPT) ensemble at each temperature. Cell parameters were taken from these runs. After the initial equilibration, a separate trajectory of 10 ns duration was generated at each temperature in the NVT ensemble to compute several equilibrium properties. The variation in cell parameters and change in cell volume with temperature (at different phases) are displayed in

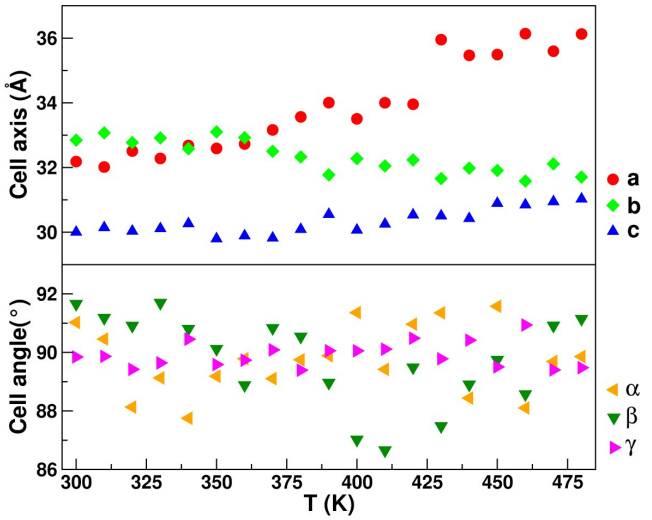

Fig. 1 Cell parameters as a function of temperature in perfect crystalline model: Cell axes (upper) and cell angles (lower). Standard deviations in cell lengths and angles are 0.15 Å and 0.62° respectively.

Fig. 1 and **Fig.** 2, respectively. We present a discussion on the identification of different phases on **Fig.** 2 later.

Vacancy model simulations: The vacancy model required a large supercell dimension (8x6x2) consisting of 384 ion pairs (9984 atoms). One pair of cation and anion was removed in order to create vacancy sites. An energy minimized configuration was used to perform simulation in NVT ensemble with a heating rate of 1 K/50 ps to obtain a configuration at 500 K. It was followed by an another equilibration of 5 ns in a fully flexible NPT ensemble. The subsequent production trajectory was generated in NVT ensemble for 100 ns to compute dynamic properties. Other simulation details were kept similar to the perfect crystalline system.

Free energy calculations: To calculate the free energy barrier of hopping of an ion to a neighbouring vacancy site, a large supercell (8x6x2) from the experimental[11] crystal structure was considered. Following an energy minimization, MD simulation in the NVT ensemble was performed; later the system was warmed up to 500K at a heating rate of 1 K/50 ps. At 500K, the system was equilibrated for over 5 ns in the fully flexible NPT ensemble. A further equilibration was carried out in the NVT ensemble for 1 ns. From this equilibrated configuration, a pair (non-adjacent) of cation and anion was chosen whose time average center of mass (COM) positions were calculated over a duration of 500 ps. The selected pair of ions were then removed and a non-interacting dummy atom was placed at those average COM positions which acted as reference locations of the vacancy site. The COM of four ions (two cations and two anions) arbitrarily chosen such that they were

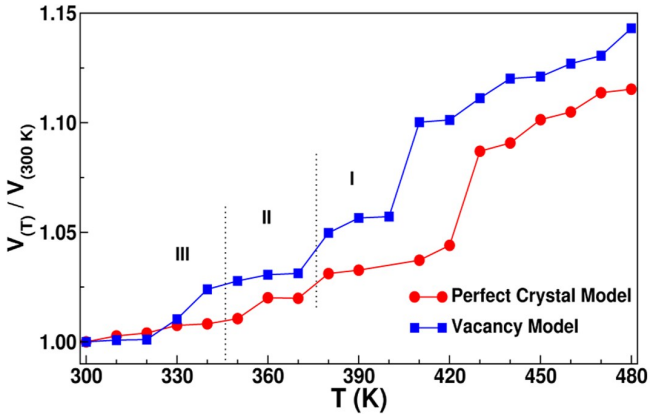

Fig. 2 Variation in the volume of simulation cell with temperature.

situated far away from a chosen vacancy site were constrained such that the whole system cannot translate during the simulation. Colvar style "distance Z" was used in determining the free energy profile using the Adaptive Biasing Force (ABF) method.[33] Reaction coordinate (RC) was defined as the distance between the COM of an ion (cation or anion) and the COM of dummy atom (See **Fig.** S2). Typically, the closest ion to the vacancy site was chosen as the "hopping" ion. ABF forces were applied every 500 steps with a bin width of 0.2 Å. An average sampling ratio was around 4 after 5 ns between the highest and lowest points. The same procedure was applied to five different initial configurations for both the ion types. Free energy profiles were calculated from these five initial configurations and are presented in **Fig.** S3. The mean free energy profile is presented and discussed later.

The effect of temperature on the vibrational spectrum was investigated through normal-mode analysis (NMA) at the harmonic level. For this, configurations collected from the classical MD trajectory at different temperatures were energy minimized in LAMMPS.[27] Later, the Hessian matrix (second derivative of the potential energy with respect to the atom coordinates) of such configurations was constructed using a normal-mode analysis code developed earlier in our group.[34] Within the harmonic approximation, diagonalization of this matrix yields eigenvectors which are proportional to atomic displacements of different modes. Complete details of charge calculations and normal-mode analysis (NMA) are provided in SI.

3 Results and Discussion

The structural characteristics of [TAZ][pfBu] at different temperatures were examined through cation-anion radial distribution functions (RDFs) (See **Fig.** S4 of SI). The H_N-O and H_C-O RDFs show that the strong N-H$\cdots$O and weaker C-H$\cdots$O hydrogen bonding interactions are not much influenced by temperature. The number of H_N atoms within the first solvation shell of oxygen atoms of anion decreases with increasing temperature, shown in **Fig.** 3 . As there are three hydrogen

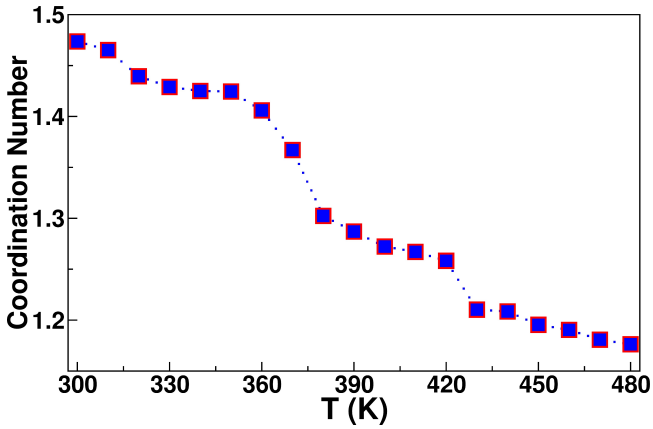

Fig. 3 Coordination number of cation's N-H hydrogen (H_N) around anion's oxygen as a function of temperature.

bonding sites on the anion and only two on the cation, the latter's rotation at intermediate temperatures allows the breakage of existing h-bonds and formation of new ones. In this manner, every oxygen site on the anion participates in hydrogen bonding, creating a dynamic 3-dimensional hydrogen bonding network. The overall decrease in the coordination number suggests the presence of disorder at higher temperature. While the ion-ion RDFs at high temperature retain most features of those at low temperatures, a few critical shoulders (sub-peaks) are missing, pointing to a loss of certain degree of crystallinity. Crucially, the triazolium rings are seen to be misoriented with increasing temperature, although they retain their lattice positions. (**Fig.** S5 of SI). Such an intermediate phase between 380 K and 430 K can thus be called as the rotator phase.

Ring plane rotational correlation (C(t)): The rotational dynamics of the cation was investigated using the time autocorrelation function of its ring normal, C(t) defined as,

$$C(t) = \langle \vec{R}_i(t).\vec{R}_i(0) \rangle \quad (1)$$

where $\vec{R}_i(t)$ is the normal vector corresponding to each 1,2,4-triazolium ring plane at time t and the function is averaged over initial times and cation indices. **Fig.** 4 shows that C(t) does not decay much at 300 K. At low temperature (phase III, **Fig.** 2), the ring planes of cations are oriented in a perfect manner as shown in **Fig.** 5a. Between 360 K and 380 K, the rate of decay increases sharply (phase II, **Fig.** 2). Above 430 K, (phase I, **Fig.** 2) the correlation function decays to zero within 0.05 ns. Cations in the lattice lose their orientational rigidity in the temperature range of 330-380 K, above which

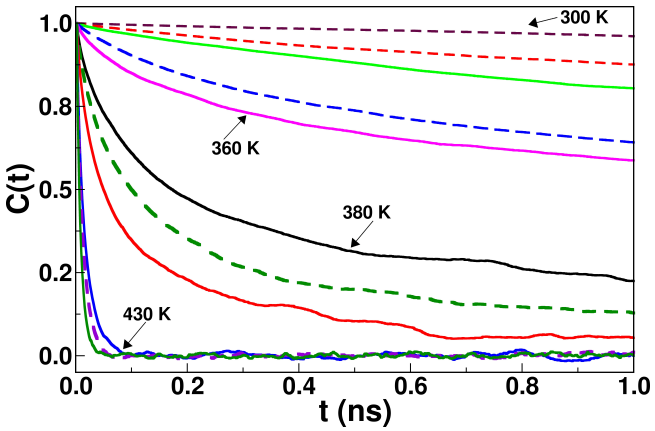

Fig. 4 Auto time correlation function of ring plane normal of the cation at different temperatures. Only a few lines are marked with temperature for the sake of clarity, unmarked lines correspond to intermediate temperatures.

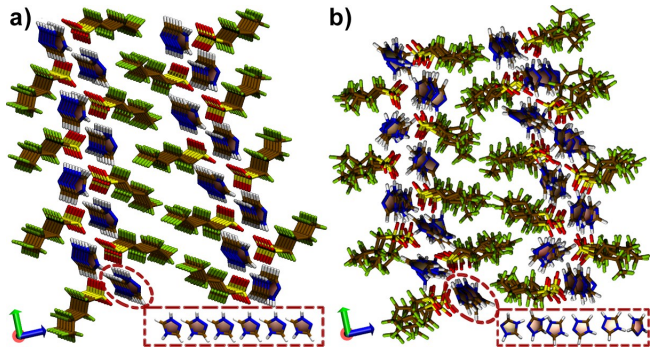

Fig. 5 Snapshots of [TAZ][pfBu] from NVT production runs at a) 330 K, and b) 380 K [carbon-ochre, nitrogen-blue, oxygen-red, fluorine-green, and sulfur-yellow (Licorice view)].

they are free to rotate which is also seen in **Fig.** 5 and **Fig.** S5 of SI. Thus, the orientational order between 1,2,4-triazolium ring planes get decorrelated at higher temperature. The ring starts rotating above 350 K and tumbles at $\sim$ 430 K.

The distribution of the angle between the ring planes of neighboring cations was calculated at different temperatures. **Fig.** 6 shows it to be sharply peaked at low temperatures with values around ± 1, implying the parallel orientation of such planes. At high temperatures, a nearly uniform distribution is seen which points to complete orientational disorder. The onset of this disorder can be captured by plotting the area under the curve (A) (between $cos(\theta)$ values of -1.0 to -0.7 and 0.7 to 1.0) against temperature as shown in inset of **Fig.** 6. Its behavior is similar to that of the dependence of volume on T (See **Fig.** 2 and **Fig.** S6 of SI), however the transitions are more evident. The observed discontinuities in both this area and the cell volume at the phase transitions are in excellent agreement with experiments [11], as expected for the three

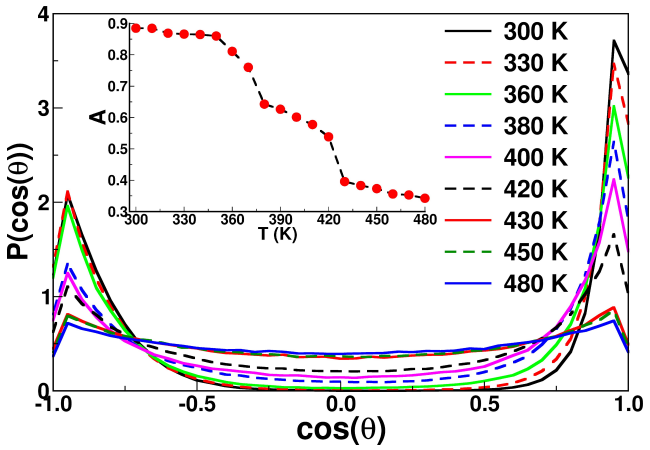

Fig. 6 Distribution of the angle between ring planes of neighboring cations. Inset: Area under the distribution, for the regions $|\cos\theta| > 0.7$ versus temperature.

phases (phases III, II and I) of [TAZ][pfBu] POIPC, although the transition temperatures seen in simulations are higher, due to superheating effects. Thus, in the simulations, the crystal is in the rotator phase at temperatures higher than 420-430 K too, and phase I of simulations is a metastable one.

Further, the vibrational density of states (VDOS) of [TAZ][pfBu] was calculated at various temperatures from the Fourier transform of the velocity time autocorrelation function of the ions (See **Fig.** S8 of SI). An increase in temperature results in the softening of modes present below 100 cm^{-1} and around 700 cm^{-1}. The former can be assigned to librations of cations and the latter to out-of-plane motion of N–H protons in triazolium cation (See **Fig.** 7). Rotational disorder at higher temperature facilitates cation mobility and thus causes the change in spectral behaviour. These observation reproduces the experimental results of Luo *et al.* [11] using [TAZ][pfBu] POIPC.

The dynamics of breakage and re-formation of cation-anion hydrogen bonds can be studied through time correlation functions. Two such TCFs, $S_{HB}(t)$ and $C_{HB}(t)$ can be defined [35–38], the former providing a measure of the life time of a hydrogen bond while the latter measures the same, but allows for the reformation of hydrogen bond between the same donor-acceptor pair. Geometric criteria to determine the presence of a h-bond and definitions of these h-bond life time correlation functions are provided in SI.

Fig. 8 displays the decay of $S_{HB}(t)$ and $C_{HB}(t)$ at different temperatures. $S_{HB}(t)$ relaxes quite fast even at 300 K due to the fast bond vibrational and librational motions of the ions. With increasing temperature, the decay rate increases. However, $C_{HB}(t)$ exhibits rapid oscillations at 300 K and decays to a constant value. The long time value of $C_{HB}(t)$ decreases with increasing temperature. At low temperatures, the prob-

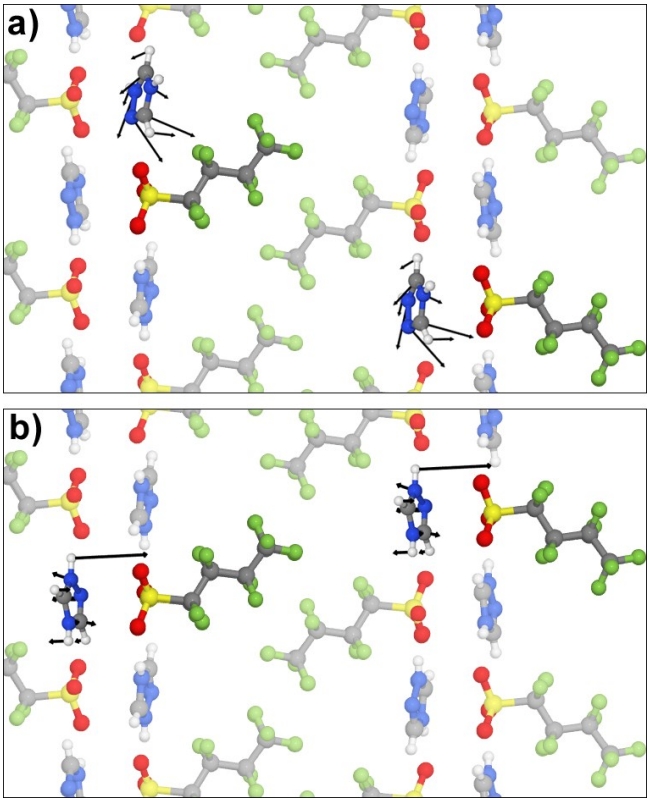

Fig. 7 Atomic displacements obtained from a normal mode analysis of crystalline POIPC. Two modes are shown for illustrative purposes. (a) librational mode of triazolium cation at 100 cm^{-1}, and (b) out-of-plane motion of N–H proton of triazolium cation at 715 cm^{-1}. Only a few ions from the modeled crystal are shown for the sake of clarity. Arrows are atomic displacements and are scaled by an arbitrary factor for better visualization. Color scheme: N - blue, C - gray, H - white, S - yellow, O - red, and F - green.

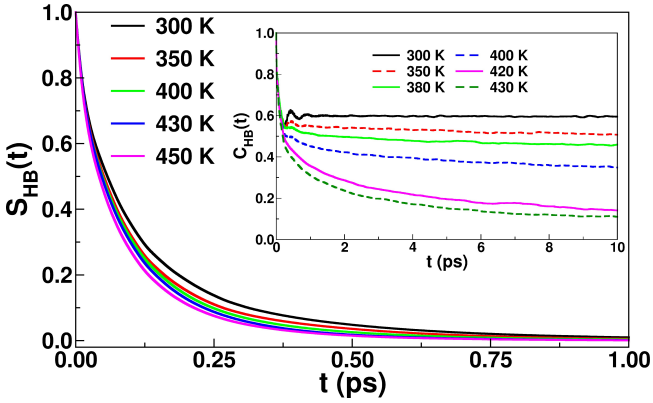

Fig. 8 Relaxations of $S_{HB}(t)$ and $C_{HB}(t)$ (see inset) h-bond lifetime correlation function, for N-H···O hydrogen bonding in POIPC.

ability for reformation of a h-bond is high and the non-zero asymptotic value of $C_{HB}(t)$ reflects this fact. At temperatures between 400 K and 430 K, this function decays slowly. The lifetime correlation functions were fitted to multi-exponential functions so as to obtain a mean relaxation time. The fit parameters are tabulated in **Table** S3 and **Table** S4 of SI, respectively. The mean lifetime obtained from $S_{HB}(t)$ is around 100 fs. Anion rotation has been suggested to assist proton hopping in POIPC crystal[11]. The short lifetime of the h-bond TCF in the plastic crystalline phase of this POIPC supports this mechanism. Further, the temperature dependence of hydrogen bond lifetime and rotational time are compared in **Fig.** 9 and interestingly, both of them were found to obey an Arrhenius behaviour. A linear fit of the time constants to inverse temperature yields the associated activation energy of individual events. As expected, the faster hydrogen bond lifetime possess a lower activation barrier (1.75 kcal/mol) than the slower rotational time (6.78 kcal/mol).

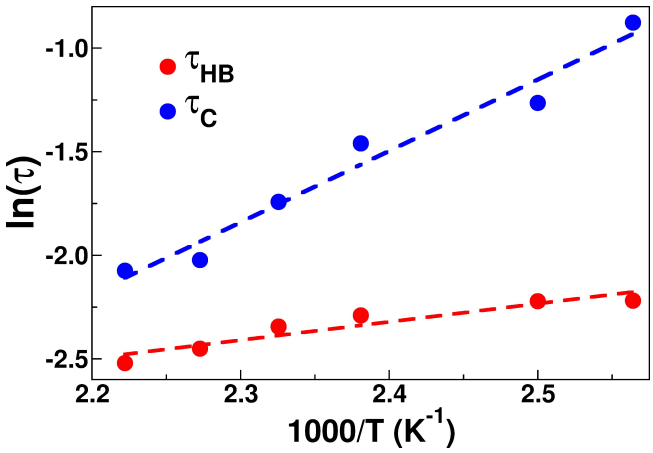

Fig. 9 Temperature dependence of hydrogen bond lifetime (τ_{HB}) and rotational time (τ_C). Dashed lines are best fits.

In the IL crystal, each ion is surrounded by its counterions forming a cage. Time averaging of ion positions permits visualization of the underlying translational order in the crystal due to the effective "removal" of vibrational disorder. The same is shown in **Fig.** 10. The average positions of the ring center at 300 K and 475 K are nearly identical, implying the invariance of translational order with temperature over this range. The mean squared displacement (MSD) of cations is also shown. After the initial ballistic motion ($\sim$ 0.2 - 0.7 ps), the MSDs of cations exhibit a plateau region (MSD $\sim$ 0.3 - 0.4 $Å^2$) due to the "cage". The plateau are very clearly seen at low temperatures. The time over which an ion is trapped inside a cage is different for cations and anions. Cations escape from the cage sooner due to their smaller size and rotational barrier,[24] compared to the anion (See **Fig.** S9 of SI

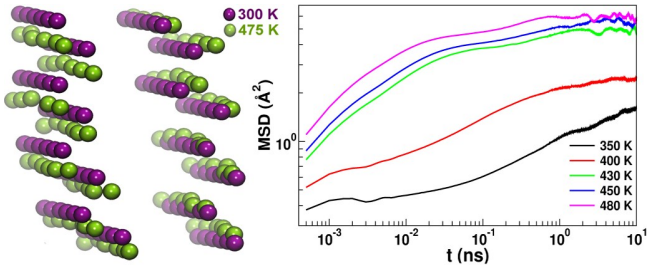

Fig. 10 Time averaged positions of cation ring center at 300 K and 475 K (left); and its mean square displacement.

which presents the MSD of cation and anion at various temperatures).

The van Hove self-correlation functions identify the nature of translation of ions as either due to hopping or diffusion[39]. Even within the diffusive regime, they can aid in identifying dynamical heterogeneity.[25,40–42] The same for the ions were calculated at 500 K, 550 K and 600 K between 0.25 to 1 ns time regime and are shown in **Fig.** 11. The first peak position for anions are slightly larger than that for cations. At 550 K, a short second peak at around 6 Å (first neighboring distance of ions) is seen at a time duration of 1 ns. The peak height grows gradually between 550 K and 600 K within 0.75 ns to 1 ns time scale. As discussed earlier, the translational motion of ions is restricted due to the formation of a cage by the counterion. The emergence of the second peak in $G_s(r,t)$ implies cation hopping. In a perfect crystal (as is the case studied here), migration of ions is possible only due to fluctuations in their environment. In the present instant, the latter is aided by rotational disorder discussed earlier. Rotational disorder aids in the migration of ions to their neighboring sites through the available free space due to structural relaxation. Cations attempting to hop to a neighboring site to later revert back to their original position, were also observed in movies of trajectories.

Ion transport in a crystalline solid state is primarily aided through defects, chief of which would be vacancies. Their concentration would increase with temperature. It is thus important to study the ion hopping phenomenon in the presence of vacancies. To this end, we have performed simulations of the crystal at 500 K which contained 384 ion pairs and one vacancy each of cation and anion. The van Hove correlation function calculated at 500 K for such a vacancy model shows the hopping of cation to take place within 1 ns time scale which was not observed in the perfect crystal (see **Fig.** 11). Thus, as expected, ion hopping occurs at a much lower temperature due to the presence of vacancies. The decay of the ring plane normal rotational correlation is much faster in the presence of vacancies compared to the perfect crystal (See **Fig.** S10 of SI) which suggests that the rotational disorder occurs at a lower temperature due to vacancies.

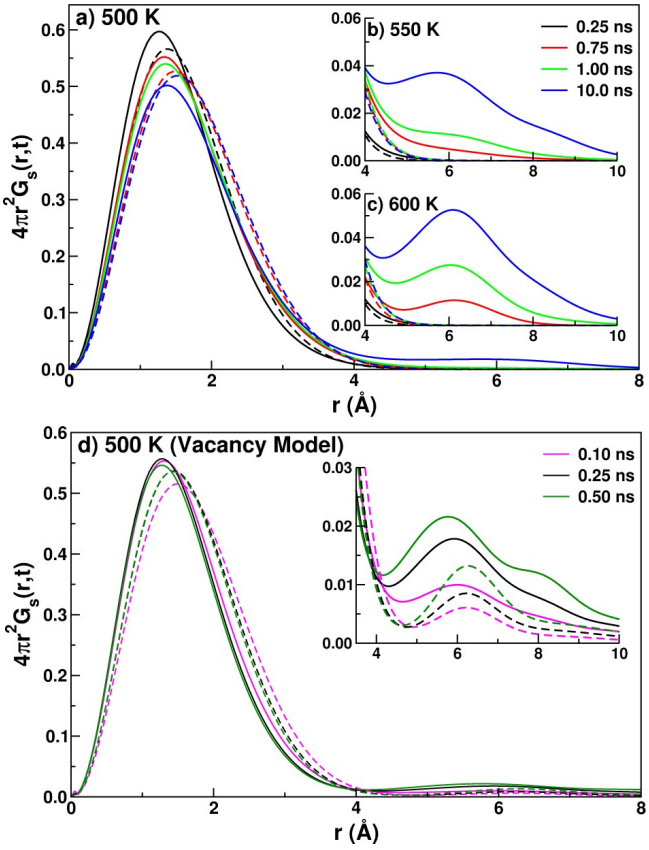

Fig. 11 Self part of van Hove correlation functions calculated for a perfect crystalline lattice from MD simulations at (a) 500 K, (b) 550 K, (c) 600 K, and using the vacancy model at (d) 500 K (solid line - for cation and dashed line - for anion).

Fig. 12(a-c) is a pictorial view depicting the concerted hopping of cations which results in a one-dimensional vacancy motion along the crystallographic b-axis. Similar to the cations, a concerted hopping of the anions is shown in **Fig.** S11 of SI. Qualitative observations showed that the hop rate for cations was higher than that for the anions. We have performed free energy calculations at 500 K to obtain the barrier associated with the hopping of ions. The calculated activation energy barrier are found to be 2.5 kcal/mol and 6.0 kcal/mol for cations and anions respectively (see **Fig.** 12(d)). Thus, a large energy barrier restricts the hopping of anions. Free energy calculations at a lower temperature of 400 K, but still within Phase I, yields larger barrier heights of 4.5 and 9.2 kcal/mol for the two ions. The activation (E_a) barrier obtained from ionic conductivity experiments in Phase I (373-430 K) was found to be 8.77 kcal/mol[11]. Although the results from simulations are able to predict the order of magnitude of E_a, there exists differences between the simulations and the experiment[11]. This could be due to the fact that the measured ionic conductivity in experiment is primarily pro-

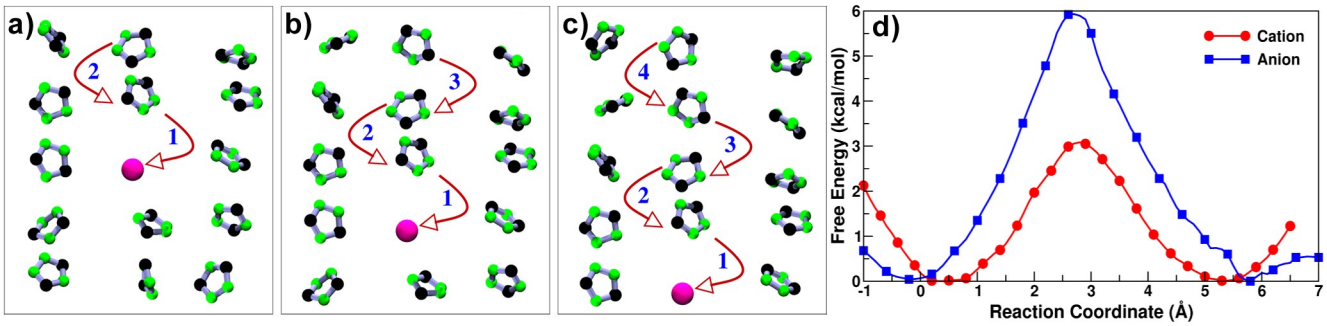

Fig. 12 (a-c) Concerted hopping of cations and (d) calculated free energy profiles for the motion of cation and anion at 500 K. Estimated standard error on the mean in the simulated free energy is around 0.22 kcal/mol.

tonic in nature, while the calculated activation energy from simulations is solely from individual ion motion i.e. cation and anion movement. Further, an estimation of ion hopping frequencies and the corresponding jump diffusion coefficients was obtained using these free energy barriers associated with the motion of cations and anions. A detailed discussion of the same is provided in SI.

4 Conclusions

In conclusion, we have identified the existence of a rotator phase in [TAZ][pfBu] POIPC. It is characterized by the decorrelation of the orientation of cation ring planes. In the plastic crystalline phase, ion rotation leads to a short life-time of the N-H$\cdots$O hydrogen bond. The same has been characterized via h-bond lifetime correlation functions. The rotational disorder also allows for the hopping of ions at higher temperatures. The disorder and consequent ion hopping are accelerated due to vacancies in the crystal, and thus occur at lower temperatures (by at least 20 K) than in a perfect crystal. As the heating rates employed here are much higher than those used in experiments, superheating is likely; the same would be reflected in higher values of temperatures of phase transitions in simulations when compared to experiments. One-dimensional vacancy motion has been delineated and the free energy barrier for ion hopping has been estimated to 2.5 and 6.0 kcal/mol for cations and anions respectively. It will be interesting to extend these atomistic simulations to investigate the diffusion of additional ionic species like small alkali ions in such POIPC, as well as to study proton diffusion using *ab initio* MD methods.

5 Acknowledgement

AM thanks JNCASR for financial support. AM thanks Karteek Kumar Bejagam for assistance in free energy calculations. APS acknowledges DST for the INSPIRE Faculty Award (DST/INSPIRE/IFA-14-MS31) and Central University of Haryana for financial support. SB thanks Sheikh Saqr Laboratory, JNCASR for a senior fellowship.

References

1 D. R. MacFarlane, J. Huang and M. Forsyth, *Nature*, 1999, **402**, 792–794.
2 P.-J. Alarco, Y. Abu-Lebdeh, A. Abouimrane and M. Armand, *Nat. Mater.*, 2004, **3**, 476–481.
3 S. J. Pas, J. M. Pringle, M. Forsyth and D. R. MacFarlane, *Phys. Chem. Chem. Phys.*, 2004, **6**, 3721–3725.
4 J. M. Pringle, P. C. Howlett, D. R. MacFarlane and M. Forsyth, *J. Mater. Chem.*, 2010, **20**, 2056–2062.
5 V. Armel, D. Velayutham, J. Sun, P. C. Howlett, M. Forsyth, D. R. MacFarlane and J. M. Pringle, *J. Mater. Chem.*, 2011, **21**, 7640–7650.
6 V. Armel, M. Forsyth, D. R. MacFarlane and J. M. Pringle, *Energy Environ. Sci.*, 2011, **4**, 2234–2239.
7 L. Jin, K. M. Nairn, C. M. Forsyth, A. J. Seeber, D. R. MacFarlane, P. C. Howlett, M. Forsyth and J. M. Pringle, *J. Am. Chem. Soc.*, 2012, **134**, 9688–9697.
8 Q. Li, X. Chen, J. Zhao, L. Qiu, Y. Zhang, B. Sun and F. Yan, *J. Mater. Chem.*, 2012, **22**, 6674–6679.
9 J. M. Pringle, *Phys. Chem. Chem. Phys.*, 2013, **15**, 1339–1351.
10 S. Li, L. Qiu, C. Shi, X. Chen and F. Yan, *Adv. Mater.*, 2014, **26**, 1266–1271.
11 J. Luo, A. H. Jensen, N. R. Brooks, J. Sniekers, M. Knipper, D. Aili, Q. Li, B. Vanroy, M. Wubbenhorst, F. Yan, L. Van Meervelt, Z. Shao, J. Fang, Z.-H. Luo, D. E. De Vos, K. Binnemans and J. Fransaer, *Energy Environ. Sci.*, 2015, **8**, 1276–1291.
12 Q. Li, J. Zhao, B. Sun, B. Lin, L. Qiu, Y. Zhang, X. Chen, J. Lu and F. Yan, *Adv. Mater.*, 2012, **24**, 945–950.
13 D. R. MacFarlane and M. Forsyth, *Adv. Mater.*, 2001, **13**, 957–966.
14 L. Jin, P. C. Howlett, J. M. Pringle, J. Janikowski, M. Armand, D. R. MacFarlane and M. Forsyth, *Energy Environ. Sci.*, 2014, **7**, 3352–3361.
15 P. Wang, Q. Dai, S. M. Zakeeruddin, M. Forsyth, D. R. MacFarlane, and M. Grätzel, *J. Am. Chem. Soc.*, 2004, **126**, 13590–13591.
16 J. Golding, N. Hamid, D. R. MacFarlane, M. Forsyth, C. Forsyth, C. Collins, and J. Huang, *Chem. Mater.*, 2001, **13**, 558–564.
17 M. Patel and A. J. Bhattacharyya, *Energy Environ. Sci.*, 2011, **4**, 429–432.
18 L. Jin, S. de Leeuw, M. V. Koudriachova, J. M. Pringle, P. C. Howlett, F. Chen and M. Forsyth, *Phys. Chem. Chem. Phys.*, 2013, **15**, 19570–19574.
19 M. Forsyth, T. Chimdi, A. Seeber, D. Gunzelmann and P. C. Howlett, *J. Mater. Chem. A*, 2014, **2**, 3993–4003.
20 F. Chen, J. M. Pringle and M. Forsyth, *Chem. Mater.*, 2015, **27**, 2666–2672.

21 C. Shi, S. Li, W. Zhang, L. Qiu and F. Yan, *J. Mater. Chem. A*, 2013, **1**, 13956–13962.

22 Q. Dai, D. R. MacFarlane, P. C. Howlett and M. Forsyth, *Angew. Chem. Int. Ed.*, 2005, **44**, 313–316.

23 K. Romanenko, J. M. Pringle, L. A. O'Dell and M. Forsyth, *Phys. Chem. Chem. Phys.*, 2015, **17**, 18991–19000.

24 F. Chen, L. Jin, S. W. de Leeuw, J. M. Pringle and M. Forsyth, *J. Chem. Phys.*, 2013, **138**, 244503.

25 F. Chen, S. W. de Leeuw and M. Forsyth, *J. Phys. Chem. Lett.*, 2013, **4**, 4085–4089.

26 L. Vilčiauskas, M. E. Tuckerman, G. Bester, S. J. Paddison and K.-D. Kreuer, *Nat. Chem.*, 2012, **4**, 461–466.

27 S. Plimpton, *J. Comput. Phys.*, 1995, **117**, 1–19.

28 C. Cadena and E. J. Maginn, *J. Phys. Chem. B*, 2006, **110**, 18026–18039.

29 S. S. Jang, V. Molinero, T. Cagin and W. A. Goddard, *J. Phys. Chem. B*, 2004, **108**, 3149–3157.

30 J. Hutter, M. Iannuzzi, F. Schiffmann and J. VandeVondele, *Wiley Interdiscip. Rev. Comput. Mol. Sci.*, 2014, **4**, 15–25.

31 T. A. Manz and D. S. Sholl, *J. Chem. Theory Comput.*, 2010, **6**, 2455–2468.

32 T. A. Manz and D. S. Sholl, *J. Chem. Theory Comput.*, 2012, **8**, 2844–2867.

33 E. Darve, D. RodríguezGómez and A. Pohorille, *J. Chem. Phys.*, 2008, **128**, 144120.

34 M. Krishnan and S. Balasubramanian, *Phys. Rev. B*, 2003, **68**, 064304.

35 D. Rapaport, *Mol. Phys.*, 1983, **50**, 1151–1162.

36 A. Luzar and D. Chandler, *Nature (London)*, 1996, **379**, 53.

37 A. Chandra, *Phys. Rev. Lett.*, 2000, **85**, 768–771.

38 S. Balasubramanian, S. Pal and B. Bagchi, *Phys. Rev. Lett.*, 2002, **89**, 115505.

39 S. Balasubramanian and K. J. Rao, *J. Phys. Chem.*, 1994, **98**, 10871–10880.

40 S. S. Sarangi, W. Zhao, F. Müller-Plathe and S. Balasubramanian, *ChemPhysChem*, 2010, **11**, 2001–2010.

41 S. M. Urahata and M. C. C. Ribeiro, *J. Phys. Chem. Lett.*, 2010, **1**, 1738–1742.

42 H. Liu and E. Maginn, *J. Chem. Phys.*, 2011, **135**, 124507.